BIOLOGICAL CRYSTALLOGRAPHY
ISSN 1399-0047

Structural study of the X-ray-induced enzymatic reaction of octahaem cytochrome *c* nitrite reductase

A. A. Trofimov,[a,b]* K. M. Polyakov,[a,b] V. A. Lazarenko,[a,c] A. N. Popov,[d] T. V. Tikhonova,[b] A. V. Tikhonov[b] and V. O. Popov[b]

[a]Engelhardt Institute of Molecular Biology, Russian Academy of Sciences, ul. Vavilova 32, Moscow 119991, Russian Federation, [b]Bach Institute of Biochemistry, Russian Academy of Sciences, Leninskii pr. 33, Moscow 119071, Russian Federation, [c]NRC Kurchatov Institute, 1 Akademika Kurchatova pl., Moscow, 123182, Russian Federation, and [d]European Synchrotron Radiation Facility, BP-220, 38043 Grenoble, France. *Correspondence e-mail: burayatina@gmail.com

Received 19 September 2014
Accepted 12 February 2015

Edited by V. Y. Lunin, Russian Academy of Sciences, Russia

Keywords: octahaem cytochrome *c* nitrite reductase; *Thioalkalivibrio nitratireducens*.

PDB references: TvNiR, free form, low-dose data set, 4q0t; medium-dose data set, 4q17; high-dose data set, 4q1o; nitrite complex, low-dose data set, 4l38; first medium-dose data set, 4l3x; second medium-dose data set, 4l3z; high-dose data set (NO complex), 4l3y; sulfite complex, low-dose data set, 4q4u; medium-dose data set, 4q5c; high-dose data set, 4q5b

Supporting information: this article has supporting information at journals.iucr.org/d

Octahaem cytochrome *c* nitrite reductase from the bacterium *Thioalkalivibrio nitratireducens* catalyzes the reduction of nitrite to ammonium and of sulfite to sulfide. The reducing properties of X-ray radiation and the high quality of the enzyme crystals allow study of the catalytic reaction of cytochrome *c* nitrite reductase directly in a crystal of the enzyme, with the reaction being induced by X-rays. Series of diffraction data sets with increasing absorbed dose were collected from crystals of the free form of the enzyme and its complexes with nitrite and sulfite. The corresponding structures revealed gradual changes associated with the reduction of the catalytic haems by X-rays. In the case of the nitrite complex the conversion of the nitrite ions bound in the active sites to NO species was observed, which is the beginning of the catalytic reaction. For the free form, an increase in the distance between the oxygen ligand bound to the catalytic haem and the iron ion of the haem took place. In the case of the sulfite complex no enzymatic reaction was detected, but there were changes in the arrangement of the active-site water molecules that were presumably associated with a change in the protonation state of the sulfite ions.

1. Introduction

The current experimental facilities for protein X-ray crystallography enable the study of enzymatic reactions not only in the traditional way, which involves solving the structures of enzyme complexes with substrate analogues that mimic different stages of the enzymatic reaction, but also by observing the dynamics of structural changes directly in a crystal. To use this approach, first of all it is necessary to know how the enzymatic reaction could be initiated in a crystal, and secondly the crystals of the enzyme must be of extremely high quality. For enzymes that catalyze redox reactions involving metal ions with a variable oxidation state, the enzymatic reaction can be initiated in a crystal using the reducing properties of X-ray radiation.

X-ray photons interact with the atoms of a protein either elastically (forming a diffraction pattern) or in an inelastic manner (Compton scattering or the photoelectric effect). The inelastic interactions lead to radiation damage to protein crystals and to different chemical modifications of the protein molecules (Garman, 2010). Radiation damage is manifested as a decrease in the resolution of the diffraction pattern, an increase in the mosaicity of the crystal, an increase in the *B*-factor values for the data and an expansion of the unit-cell volume. Specific structural damage is manifested as disruption

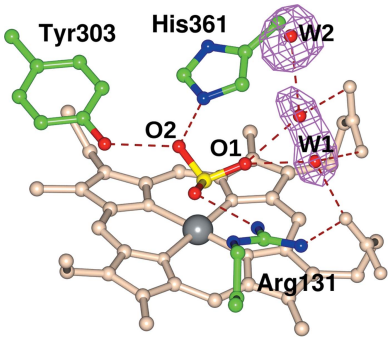

of disulfide bonds (Sutton *et al.*, 2013; Carpentier *et al.*, 2010), decarboxylation of glutamate and aspartate residues (Fioravanti *et al.*, 2007; Burmeister, 2000; Weik *et al.*, 2000), loss of the hydroxyl groups of tyrosines and the methylthio groups of methionines (Burmeister, 2000), and the reduction of some metal centres (Adam *et al.*, 2004; Beitlich *et al.*, 2007; Frankaer *et al.*, 2014). X-ray-induced reduction of metal ions in proteins is registered by single-crystal optical and X-ray absorption spectroscopies.

To date, the number of crystallographic papers devoted to the dynamics of enzymatic reactions induced by X-ray radiation is relatively small. Crystal structures corresponding to different total doses of absorbed radiation have been used to investigate the X-ray-induced four-electron reduction of dioxygen in the active site of horseradish peroxidase (Berglund *et al.*, 2002). A series of five structures made it possible to observe the breakage of the O—O bond in the initial dioxygen complex of the enzyme (leading to the formation of a 'ferryl-like' species and a water molecule), the formation of the second water molecule from the 'ferryl-like' species and its dissociation. An analogous X-ray-induced breakage of the O—O bond in the oxygen molecule was also observed in structures of complexes of reduced cytochrome P450cam (Schlichting *et al.*, 2000) and cytochrome cd_1 (Sjögren & Hajdu, 2001). Partial reduction of the dioxygen complex occurs even at the minimal absorbed dose required to obtain a statistically significant data set (Berglund *et al.*, 2002). It was shown by Beitlich *et al.* (2007) that at a dose of 0.5 MGy the structure of chloroperoxidase already corresponds to the partially reduced enzyme. In these studies (Sjögren & Hajdu, 2001; Berglund *et al.*, 2002; Beitlich *et al.*, 2007), a complete set of diffraction data for the lowest possible dose was obtained by combining partial low-dose data sets collected from several crystals. Recently, Komori *et al.* (2014) managed to observe gradual changes in the coordination spheres of the catalytic copper ions of a multicopper oxidase owing to reduction of the copper ions by X-ray radiation; here, one protein crystal was used to collect data for the whole series and the minimal possible dose was reduced by translating the crystal several times during data collection.

Structures of the octahaem cytochrome *c* nitrite reductase from the bacterium *Thioalkalivibrio nitratireducens* (TvNiR; Tikhonova *et al.*, 2006; Polyakov *et al.*, 2009) and its substrate complexes (Trofimov *et al.*, 2010, 2012) have been solved previously. The structure of TvNiR is similar to that of pentahaem cytochrome *c* nitrite reductase (NrfA; Einsle *et al.*, 1999). The active sites of TvNiR and NrfA are formed by structurally conserved catalytic histidine, tyrosine and arginine residues (His361, Tyr303 and Arg131 in TvNiR) and the lysine-coordinated haem *c*. Based on the structures of NrfA complexes with substrates (nitrite and hydroxylamine) and model quantum-chemical calculations, a mechanism for the six-electron reduction of nitrite to ammonium has been proposed for NrfA (Einsle *et al.*, 2002). It should be noted that for crystalline NrfA the X-ray-induced reduction of haems was shown spectrophotometrically and without assessment of the dose (Kemp *et al.*, 2010).

In this study, the X-ray-induced enzymatic reaction of cytochrome *c* nitrite reductase was investigated using a series of diffraction data sets collected from crystals of the free form of the enzyme and its substrate complexes (nitrite and sulfite) with a gradual increase in the total dose of absorbed X-ray radiation. The high quality of TvNiR crystals allows complete diffraction data sets to be collected to resolutions of better than 2 Å with absorbed doses not exceeding 0.3–0.4 MGy. Previously, TvNiR was shown to be highly resistant to radiation damage at room temperature, and it has been suggested that TvNiR might catalyze the conversion of one or several water radiolysis products to water (Leal *et al.*, 2013).

2. Materials and methods

2.1. Crystallization and preparation of the complexes

Crystals of TvNiR were grown by the hanging-drop vapour-diffusion method. The drops consisted of equal volumes (2.5 µl) of the protein and reservoir solutions. The protein solution consisted of 10.0 mg ml^{-1} TvNiR, 50 m*M* Tris–HCl pH 7.2. The reservoir solution consisted of 1.26 *M* trisodium citrate, 90 m*M* HEPES–NaOH pH 7.5, 10%(*v*/*v*) glycerol (condition 1) or 0.2 *M* ammonium acetate, 0.1 *M* sodium citrate tribasic pH 5.6, 30%(*v*/*v*) 2-methyl-2,4-pentanediol, 50 m*M* sodium sulfite (condition 2; sulfite complex of TvNiR).

The crystals of the free form of TvNiR were grown using condition 1. The nitrite complex of TvNiR was obtained by soaking a protein crystal from condition 1 in a solution containing 50 m*M* sodium nitrite for 10 min.

2.2. Data collection and processing

The crystals of TvNiR belonged to the cubic space group $P2_13$ and had an equidimensional rhombic dodecahedral habit; the unit-cell parameter for the crystal of the free form is 195.48 Å. The crystal sizes were around 150–200 µm. The crystals were mounted directly from the solution using large nylon loops and were cryocooled in a nitrogen-gas stream at 100 K (Oxford Cryostream 600).

The diffraction measurements (Table 1) were carried out at the European Synchrotron Radiation Facility (ESRF). The absorbed dose rate was estimated with *RADDOSE* (Paithankar *et al.*, 2009) using the photon flux values obtained by measurements using standard calibrated intensity monitors and the chemical compositions of the protein and the crystallization solution. To plan the diffraction measurements, *BEST* (Bourenkov & Popov, 2010) was used. The standard procedure for radiation-sensitivity measurements (Leal *et al.*, 2010), as implemented in *MxCuBE*/*EDNA* (Gabadinho *et al.*, 2010; Incardona *et al.*, 2009), was applied for one of the free-form crystals in order to experimentally check the correctness of the dose-rate estimation. The data-collection strategy was selected so that the total absorbed dose per data set was minimal.

For the TvNiR–sulfite complex, 19 successive complete data sets were collected on beamline ID14-EH1 at a wavelength of 0.934 Å (13.275 keV) using an ADSC Q210 CCD detector.

Table 1
Data-collection and refinement statistics for the TvNiR data series.

Values in parentheses are for the highest resolution bin.

	Free form			Sulfite complex			Nitrite complex				
Data set	1	9	20	1	4	19	1	5	9	13	20
PDB code	4q0t	4q17	4q1o	4q4u	4q5c	4q5b	4l38	4l3x	4l3z	4l3y	—
Total dose (MGy)	0.15	1.39	3.08	0.48	1.45	6.26	0.24	1.20	2.16	3.12	4.80
Resolution (Å)	1.70 (1.80–1.70)	1.70 (1.80–1.70)	1.75 (1.80–1.75)	1.62 (1.68–1.62)	1.62 (1.68–1.62)	1.74 (1.80–1.74)	1.80 (1.90–1.80)	1.85 (1.90–1.85)	1.85 (1.90–1.85)	1.95 (2.00–1.95)	2.05 (2.10–2.05)
Completeness (%)	98.8 (99.3)	99.1 (99.2)	98.9 (99.9)	98.1 (90.0)	98.1 (89.9)	99.1 (98.6)	99.4 (98.9)	99.4 (98.9)	99.4 (98.9)	99.5 (99.0)	96.6 (96.1)
Multiplicity	3.0 (3.0)	3.0 (3.0)	2.4 (2.4)	3.3 (2.5)	3.3 (2.5)	3.4 (3.4)	2.7 (2.9)	2.9 (3.1)	2.8 (2.9)	2.7 (2.8)	2.2 (2.3)
R_{meas}†	0.068 (0.527)	0.071 (0.630)	0.076 (0.618)	0.065 (0.488)	0.063 (0.502)	0.072 (0.840)	0.126 (0.670)	0.125 (0.674)	0.131 (0.803)	0.123 (0.683)	0.128 (0.728)
$\langle I/\sigma(I)\rangle$	11.7 (2.5)	10.5 (2.2)	10.1 (2.2)	13.4 (2.4)	13.8 (2.3)	12.7 (1.8)	8.6 (2.1)	8.7 (2.3)	8.3 (1.9)	7.8 (2.3)	6.8 (2.1)
$CC_{1/2}$‡ (%)	(74)	(67)	(56)	(82)	(81)	(65)	(66)	(65)	(57)	(58)	(60)
B factor (Å^2)	13.8	14.9	16.4	14.6	15.1	20.2	10.2	10.7	11.6	12.5	14.3
R	0.158	0.159	0.155	0.158	0.157	0.152	0.153	0.153	0.156	0.151	0.157
R_{free}	0.170	0.172	0.166	0.171	0.168	0.017	0.170	0.170	0.174	0.170	0.182
R.m.s.d., bonds (Å)	0.016	0.017	0.015	0.016	0.016	0.016	0.017	0.017	0.017	0.017	0.016
R.m.s.d., angles (°)	2.53	2.54	2.56	2.49	2.50	2.55	2.59	2.55	2.58	2.58	2.60
No. of water molecules	1320	1308	1173	1184	1177	958	1295	1268	1229	1211	1050
Cruickshank's DPI for coordinate error (Å)	0.066	0.066	0.065	0.053	0.053	0.067	0.070	0.075	0.076	0.086	0.105
Maximum-likelihood-based standard uncertainty of thermal parameters (Å^2)	1.2	1.3	1.4	1.0	1.0	1.4	1.4	1.6	1.7	2.0	2.6

† $R_{meas} = \sum_{hkl}\{N(hkl)/[N(hkl)-1]\}^{1/2}\sum_i |I_i(hkl) - \langle I(hkl)\rangle|/\sum_{hkl}\sum_i I_i(hkl)$, where $N(hkl)$ is the total number of times a given reflection is measured. ‡ $CC_{1/2}$ is the percentage of correlation between intensities from random half data sets (Karplus & Diederichs, 2012).

The X-ray beam was collimated with beam slits to 150 × 150 µm; the estimated dose rate was about 0.3 kGy s^{-1}. The data were collected over identical absolute rotation ranges from the same volume of the same crystal with approximate dimensions 150 × 150 × 100 µm. Each data set was collected within 744 s; the exposure time was 6.9 s per frame and the absorbed dose per set was 0.24 MGy. All data sets were collected with 0.25° oscillation in one pass over a total of 27°. The ESRF storage ring was operated at 200 mA current, the beam flux was 1.4 × 10^{10} photons s^{-1} and the estimated dose rate was about 300 Gy s^{-1}.

Diffraction measurements for the TvNiR–nitrite complex and the free form were carried out on beamline ID23-1 (Nurizzo *et al.*, 2006) using an ADSC Q315R CCD detector. The X-ray beam energy was 12.75 keV in both cases. The beam size at the sample position (the nominal FWHM spot size was 35 µm vertically and 45 µm horizontally) was tailored to a diameter of 30 µm using the corresponding aperture. The crystal dimensions were approximately 200 × 200 × 120 µm. The ESRF storage ring was operated at 30 mA current, the beam flux was 1.6 × 10^{11} photons s^{-1} and the estimated dose rate was 50 kGy s^{-1}.

The starting angle of data collection was chosen so that a 25° total rotation (for the free form and the nitrite complex) was sufficient to achieve a complete set of diffraction data. In order to obtain a higher resolution data set within a limited absorbed dose and also to exclude variation in the exposed crystal volume, the sample position relative to the beam was changed five times during data collection, with a relatively small rotation of 5° used per position and a crystal shift of 50 µm between positions. The complete procedure of data collection to a resolution of 1.7 Å, with a rotation width of 0.5° and exposure times of 0.5 and 0.27 s per image for the TvNiR–nitrite complex and the free form, respectively, was repeated 20 times for each crystal position.

The data were indexed, integrated and scaled using *XDS*/*XSCALE* (Kabsch, 2010). Overall, radiation damage leads to a reduction in the diffraction power of the crystal and was manifested as contamination of the data-collection statistics, a decrease in the maximum resolution limit and an expansion of the unit-cell volume. The resolution cutoff for each data set was chosen so that the $I/\sigma(I)$ ratio was about 2 in the last shell and the correlation coefficient $CC_{1/2}$ was greater than 0.5 (Karplus & Diederichs, 2012). Overall *B*-factor values for each serial data set were calculated by *BEST* (Bourenkov & Popov, 2010) using the intensities merged by *XDS*.

2.3. Structure refinement

A previously determined TvNiR structure (PDB entry 2ot4; Polyakov *et al.*, 2009) was used as the starting model for refinement of the first structure in each series. Each refined structure in a series was used as the starting model for the refinement of the next structure in the series. Refinement was performed using *REFMAC* (Murshudov *et al.*, 2011; Winn *et al.*, 2011). Manual corrections of the model were performed based on the analysis of difference Fourier maps using *Coot* (Emsley & Cowtan, 2004). The refinement statistics are given in Table 1.

3. Results

3.1. Overall structure and radiation damage

20 diffraction data sets were collected for both the free form of TvNiR and the nitrite complex to total absorbed doses of

3.08 and 4.80 MGy, respectively. For the sulfite complex of the enzyme, 19 data sets were collected to a dose of 6.26 MGy. All of the structures were refined crystallographically; some structures at low, medium and high doses from each series were deposited in the PDB (Table 1).

The increase in absorbed dose leads to a gradual deterioration in the resolution and to an almost linear increase in the overall *B*-factor values for the data sets, which is indicative of the absence of significant radiation damage to the protein (Owen *et al.*, 2006). The dependence of the *B* factor for our data on the absorbed dose is shown in Fig. 1. One unit of the scaling *B* factor is equivalent to about 1 MGy for all three cases, which is in a very good agreement with the well known observations published by Kmetko *et al.* (2006) and Borek *et al.* (2007) and supports the correctness of our dose measurements. No significant global changes were detected in the structures of the series with increasing dose. The structures of one series can be superimposed with r.m.s.d. values of less than 0.18 Å on all C^{α} atoms. Along with this, local changes associated with radiation damage are observed with increasing dose: the number of water molecules decreases gradually (Table 1) and some Asp and Glu residues are decarboxylated. In all three series the decarboxylation of the same residues is observed.

Decarboxylation was assessed by the increase in the individual atomic *B* factors of the side chains and by changes in the electron-density maps with increasing dose. For the sulfite complex, the decarboxylation of 20 residues was detected. In the cases of the nitrite complex and the free form of the enzyme, the number of such residues was much lower. For the free form, this is associated with the low value of the maximum total dose; for the nitrite complex, decarboxylation is poorly detected owing to the relatively low resolution. An example of decarboxylation is shown in Fig. 2 for Glu89 of the sulfite complex. It should be noted that in the TvNiR series significant decarboxylation is observed at doses higher than 3 MGy.

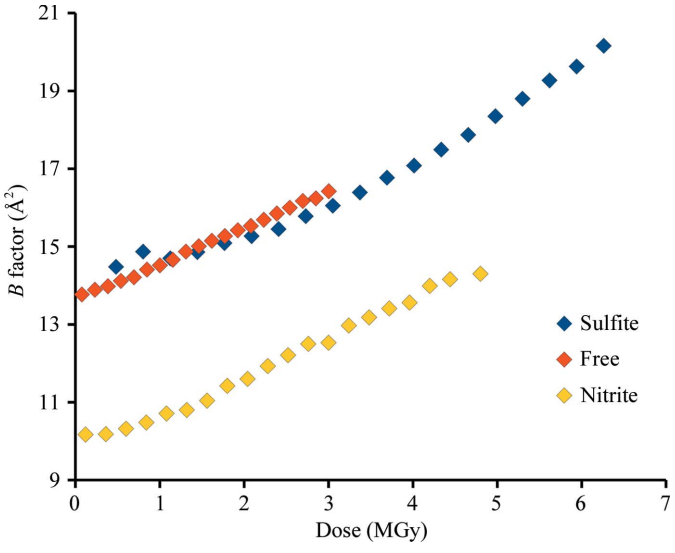

Figure 1
The dependence of the *B* factor of the data on the absorbed dose for the free form (red), the nitrite complex (yellow) and the sulfite complex (blue) of TvNiR.

3.2. Free form of TvNiR

In all of the structures in this series, an oxygen ligand (W; a water molecule/hydroxide ion) is bound to the iron ion of the catalytic haem. If the structures are refined using full occupancy for W, then the *B*-factor values for W increase faster with dose than those for the iron ion. This was interpreted as a gradual decrease in the occupancy of W. The W occupancy was adjusted manually during the crystallographic refinement so that the atomic *B* factors for W and the iron ion were approximately equal. In the structures of the series, the occupancy of W gradually decreases from 1 to 0.6, with the Fe–W distance increasing from 2.02 to 2.22 Å (Fig. 3).

3.3. Sulfite complex of TvNiR

In all the structures of this series, a sulfite ion is localized in the active site with full occupancy (Fig. 4). The sulfite forms a coordination bond to the iron ion of the haem through its S atom and forms hydrogen bonds to His361, Tyr303 and Arg131, as in previously determined structures of TvNiR complexes (Trofimov *et al.*, 2010, 2012). The dependence of the *B*-factor values for the sulfite atoms and the iron ion on dose is shown in Fig. 5. It should be noted here that the sulfite has significant asymmetry associated with higher *B*-factor values for the O1 atom compared with the other atoms.

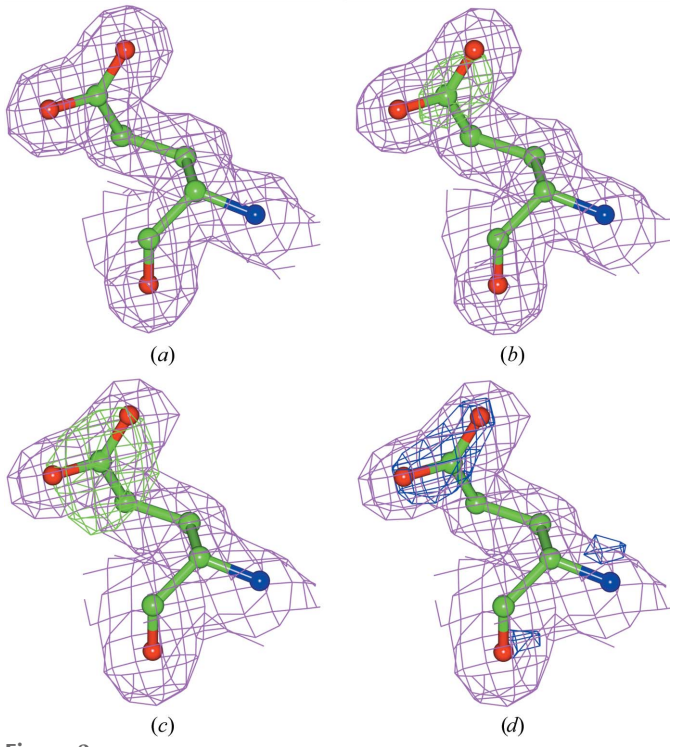

Figure 2
Decarboxylation of Glu89 in the sulfite complex of TvNiR. The corresponding total doses are (*a*) 0.48 MGy, (*b*) 2.41 MGy and (*c*, *d*) 6.26 MGy. The electron-density maps are $2F_o - F_c$ (magenta, 1σ) and $F_o - F_c$ (green, 3σ) maps and the difference map between the first and the last data sets (blue, 6σ).

In structures 1–3 of this series, a water molecule bound to the carboxyl groups of the haem (W1) has two positions with partial occupancies (Fig. 4*a*). In all of the structures of TvNiR determined previously, only one position (with full occupancy) was observed for W1, in which W1 directly forms hydrogen bonds to the two carboxyl groups of the haem. In structures 1–3 of the series, the occupancy of the main W1 position observed previously gradually increases with dose, while the occupancy of the other position decreases. The reorganization of the W1 binding occurs simultaneously with the appearance of a second position for water molecule W2 bound near the exit from the active-site cavity (Fig. 4*b*). In structure 4 (total dose of 1.45 MGy) and all subsequent structures, all W1 molecules are in the main position (with full occupancy) (Fig. 4*b*).

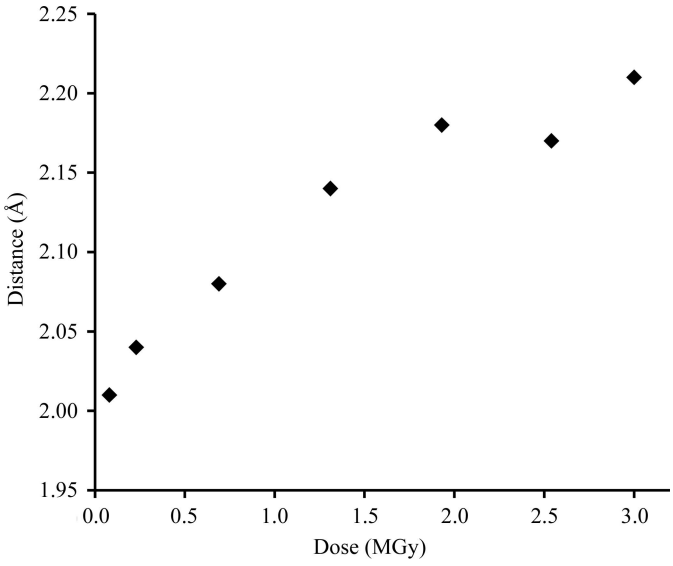

Figure 3
The dependence of the Fe–W distance on absorbed dose for the free form of TvNiR.

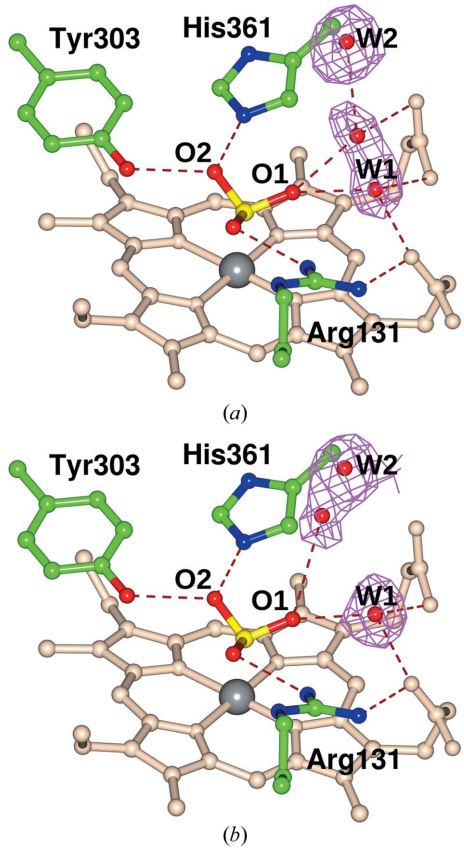

Figure 4
Sulfite complex of TvNiR. (*a*) Structure 1 (total dose 0.48 MGy). (*b*) Structure 4 (1.45 MGy). The $2F_o - F_c$ electron-density map (1σ) is shown for water molecules W1 and W2. Hydrogen bonds are indicated by dashed lines.

3.4. Nitrite complex of TvNiR

The nitrite ion forms a coordination bond to the iron ion of the haem through its N atom and forms hydrogen bonds to His361, Tyr303 and Arg131 as in previously determined structures of TvNiR complexes (Polyakov *et al.*, 2009; Trofimov *et al.*, 2012; Fig. 6*a*).

The first data set of this series was collected with the lowest possible dose (0.24 MGy), which allowed a resolution of 1.8 Å to be reached. In this structure, the electron density of the ligand in the active site is well modelled by a nitrite ion and an oxygen ligand (W) with occupancies of 0.5 (Fig. 6*a*). The *B*-factor values for the three nitrite atoms are approximately the same and are similar to the value of the *B* factor for the haem iron ion (Fig. 7).

In structures 2–13, a gradual decrease in the electron density for the O1 nitrite atom is observed (Fig. 6). This was interpreted as a gradual conversion of nitrite ions to NO induced by X-ray radiation. For structures 1–13, the occupancy of the O1 nitrite atom was adjusted manually during the

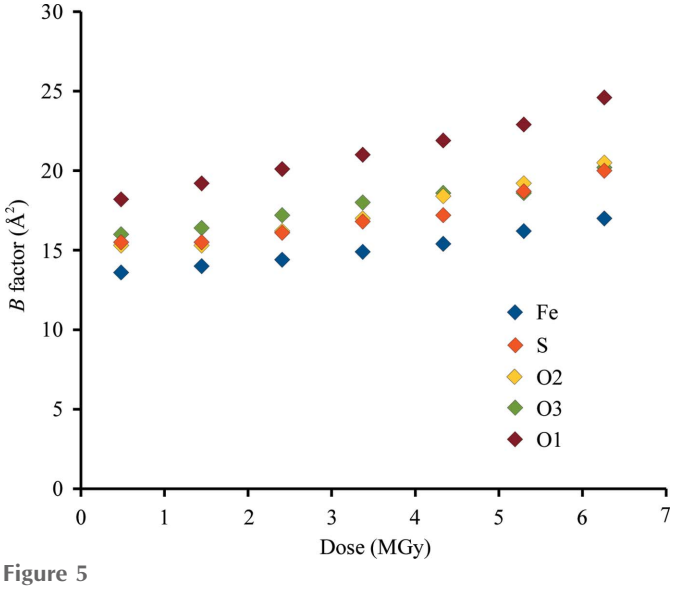

Figure 5
The dependence of the *B* factors of the sulfite atoms and the iron ion of the catalytic haem on the absorbed dose. The plots for the iron ion and the sulfite S atom are shown in blue and red, respectively. The plots for the O2, O3 and O1 sulfite atoms are shown in yellow, green and brown, respectively.

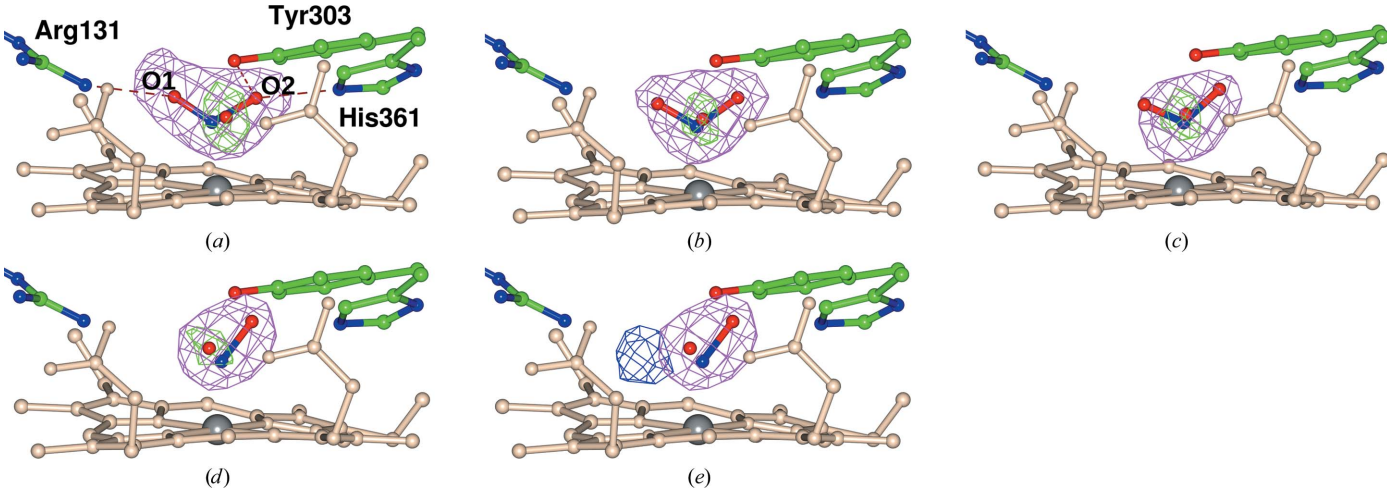

Figure 6
Nitrite complex of TvNiR. (*a*) Structure 1 (total dose 0.24 MGy). (*b*) Structure 5 (total dose 1.20 MGy). (*c*) Structure 9 (total dose 2.16 MGy). (*d*, *e*) Structure 13 (total dose 3.12 MGy). The electron density for the nitrite and W is shown in magenta (OMIT $F_o - F_c$ map for the ligands; the level corresponds to the 1σ level of the $2F_o - F_c$ map in this region), the density for W is shown in green (OMIT $F_o - F_c$ map for W contoured at the 5σ level) and the difference map between data sets 1 and 13 is in blue (6σ). Hydrogen bonds are indicated by dashed lines.

crystallographic refinement so that the *B* factors of this atom and the nitrite N atom were approximately equal. For structures 1, 5 and 9, the occupancies of the O1 nitrite atom were 0.5, 0.35 and 0.2, respectively. In structure 13 (total dose of 3.12 MGy) electron density for the O1 atom was absent. For this structure and the subsequent structures, a model consisting of a diatomic NO ligand and an oxygen ligand (with occupancies of 0.5) was used in refinement. The NO is inclined towards His361 and Tyr303, and its O atom forms two hydrogen bonds to these residues. In the previously determined structure of the hydroxylamine complex of TvNiR (PDB entry 3owm), the diatomic ligand is also inclined towards His361 and Tyr303.

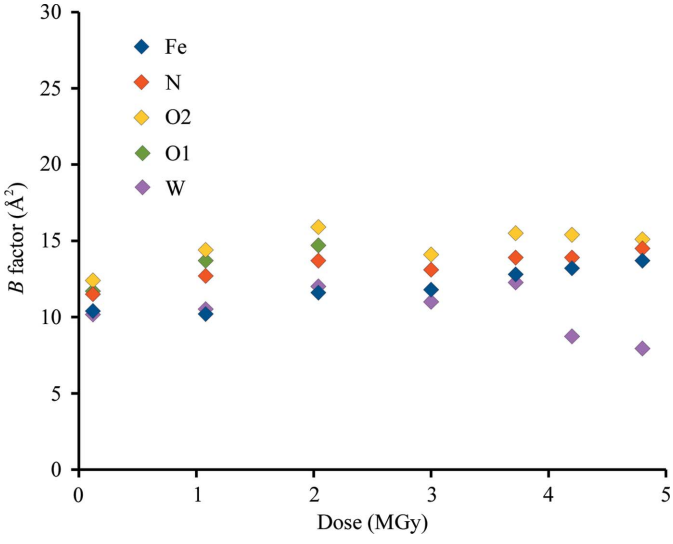

Figure 7
The dependence of the *B* factors of the nitrite atoms (the plots for the N, O2 and O1 atoms are shown in red, yellow and green, respectively), the oxygen ligand (magenta) and the iron ion (blue) on absorbed dose. In structures 1, 5 and 9 the occupancy of the O1 nitrite atom is 0.5, 0.35 and 0.2, respectively. The occupancies of the other ligand atoms are 0.5.

4. Discussion

X-ray radiation causes changes in the structure of the TvNiR active site both in the free form of TvNiR and its complexes with substrates (nitrite and sulfite).

In the case of the free form of TvNiR, a gradual increase in the distance between the iron ion of the catalytic haem and the oxygen ligand W that is bound to it takes place on increasing the dose of absorbed radiation, and the occupancy of W decreases simultaneously. For structures 1 and 2 the difference in the Fe–W distance is only 0.04 Å, which is comparable with the error in determining the coordinates of the atoms (Cruickshank's DPI for coordinate error is about 0.07 Å). However, a tendency towards an increase in this distance is apparent in the series. This increase may be associated with the degree of reduction of the catalytic haems. In the first structure, the Fe–W distance is 2.02 Å, which is consistent with the data from Einsle *et al.* (2002), in which the experimentally obtained Fe—O distance was 2.1 Å and was interpreted as the result of simultaneous binding of hydroxide ions and water molecules to the oxidized iron ions [the calculated distances for iron(III)—OH^- and iron(III)—H_2O are 1.86 and 2.26 Å, respectively]. According to Einsle *et al.* (2002), for the reduced haem the Fe—O distance is 2.39 Å. Moreover, such a complex can dissociate relatively easy. Since in structure 20 (total dose 3.08 MGy) of the TvNiR free form the Fe–W distance is 2.22 Å, it can be concluded that not all active sites of the enzyme are reduced at the corresponding total dose.

In the case of the sulfite complex of TvNiR, the catalytic reaction is not observed during X-ray irradiation of the protein up to a total dose of 6.26 MGy. Apparently, for the catalytic reduction of sulfite to start, simultaneous delivery of

several electrons to the active site is required, which is difficult when the enzyme is reduced by X-rays. In structures 1–3 of this series it was found that water molecule W1 bound to the carboxyl groups of the catalytic haem can occupy two positions (Fig. 4). These two positions can be explained by the ability of sulfite to bind both in protonated and deprotonated forms (the pK_a for HSO_3^- is 6.97). In the main position, W1 participates in the formation of three strong hydrogen bonds, with both its protons being involved in interactions with the deprotonated carboxyl groups of the haem. In this case sulfite can bind only as HSO_3^-, forming a hydrogen bond to W1 through the proton at the O1 atom. In the second position, W1 participates in the binding of the deprotonated form of sulfite, being a proton donor.

Hence, in the first three structures of the series the electron density of the sulfite should correspond to a mixture of HSO_3^- and SO_3^{2-}. The gradual reduction of the catalytic haems under X-ray radiation leads to polarization of the bonds of the SO_3^{2-} ions owing to the back-bonding effect, causing protonation of its O1 atoms. As a result of this, there is a shift of the W1 molecule from the second position to the main position, coupled with a shift of the W2 molecule to a new position (Fig. 4). In structure 4, the sulfite is in the protonated form and all W1 molecules are in the main position. It should be noted that in all of the previously determined structures of sulfite complexes of TvNiR the sulfite was bound as HSO_3^- and the corresponding crystals were partially reduced. The protonation of the O1 sulfite atom may explain the higher value of the *B* factor of this atom compared with the other sulfite atoms (Fig. 5). In the structure of the sulfite complex of TvNiR determined previously at 1.4 Å resolution (PDB entry 3fo3; Trofimov *et al.*, 2010), the asymmetry of the sulfite bound in the active site is revealed by the shape of the anisotropic ellipsoid for the O1 atom, which is rather stretched compared with the other sulfite atoms (our unpublished data).

In the case of the nitrite complex of TvNiR, in structures 1–12 (up to a total dose of 3.12 MGy) a gradual disappearance of the nitrite O atom bound to Arg131 is observed (Fig. 6). In structures 13–20 the active site of the enzyme is occupied by a diatomic NO species forming hydrogen bonds to His361 and Tyr303. This may be considered to be a result of the initial stages of the catalytic nitrite reduction induced by X-ray radiation. The absence of significant decarboxylation of Asp and Glu residues at doses below 3 MGy (Fig. 2) suggests that the disappearance of one O atom of the nitrite is not directly associated with radiation damage but is the result of the enzymatic reaction.

Based on the fact that the O atom of NO is bound to His361 and Tyr303, it can be assumed that the first nitrite O atom to be cleaved is that bound to Arg131, which corresponds to a variant of the catalysis discussed by Bykov & Neese (2012). On the other hand, elimination of the nitrite O atom forming hydrogen bonds to His361 and Tyr303 seems to be more likely because His and Tyr residues are much more effective proton donors than an Arg residue. According to the mechanism proposed by Einsle *et al.* (2002), as a result of the cleavage of the first nitrite O atom an unstable iron(II)–NO^+ intermediate is initially formed, in which the NO^+ ion is perpendicular to the plane of the haem. It is the formation of this unstable intermediate that explains the breakage of the hydrogen bond between the second O atom of the nitrite and Arg131.

In structures 13–20 of the nitrite series, no changes associated with cleavage of the second O atom of the nitrite were found in the active site. This might be owing to insufficient absorbed doses for the reaction to continue (cleavage of the second O atom of the nitrite). Another possible reason for this might be difficulties in passing the two-electron reduction stages with the enzyme being reduced by X-ray radiation.

5. Conclusion

In series of TvNiR structures, we managed to detect a gradual reduction of the catalytic haems by X-ray radiation. In the case of the free form of TvNiR, the signs of this reduction are a gradual increase in the Fe—O distance and the dissociation of the oxygen ligands bound to the catalytic iron ions on increasing the dose of radiation absorbed. In the series for the sulfite complex of TvNiR, reduction of the haems leads to protonation of the O1 atoms of the SO_3^{2-} ions bound in the active sites. This effect is revealed in the structures as a reorganization of the binding of water molecules in the active site. In the case of the nitrite complex of TvNiR, X-ray radiation induces the conversion of the nitrite ions bound in the active sites to NO, which is the beginning of the catalytic reaction. The NO species form hydrogen bonds to His361 and Tyr303, which are likely to be the major proton donors in the catalytic process.

The reduction of cytochrome *c* nitrite reductases in crystals under X-ray radiation and the relatively long diffraction data-collection times used for these crystals allow us to conclude that all previously determined structures of cytochrome *c* nitrite reductases correspond to reduced enzymes. To study the structures of the enzymes in the oxidized state, special effort must be made.

Acknowledgements

This work was supported by the Russian Scientific Foundation (Project No. 14-24-00172). KMP was supported by the 'Molecular and Cellular Biology' Program of the Russian Academy of Sciences. We acknowledge the European Synchrotron Radiation Facility for provision of synchrotron-radiation facilities (MX1641 and Radiation Damage Bag).

References

Adam, V., Royant, A., Nivière, V., Molina-Heredia, F. P. & Bourgeois, D. (2004). *Structure*, **12**, 1729–1740.
Beitlich, T., Kühnel, K., Schulze-Briese, C., Shoeman, R. L. & Schlichting, I. (2007). *J. Synchrotron Rad.* **14**, 11–23.
Berglund, G. I., Carlsson, G. H., Smith, A. T., Szöke, H., Henriksen, A. & Hajdu, J. (2002). *Nature (London)*, **417**, 463–468.
Borek, D., Ginell, S. L., Cymborowski, M., Minor, W. & Otwinowski, Z. (2007). *J. Synchrotron Rad.* **14**, 24–33.
Bourenkov, G. P. & Popov, A. N. (2010). *Acta Cryst.* D**66**, 409–419.
Burmeister, W. P. (2000). *Acta Cryst.* D**56**, 328–341.
Bykov, D. & Neese, F. (2012). *J. Biol. Inorg. Chem.* **17**, 741–760.

Carpentier, P., Royant, A., Weik, M. & Bourgeois, D. (2010). *Structure*, **18**, 1410–1419.
Einsle, O., Kroneck, P. M. H., Messerschmidt, A., Stach, P., Bourenkov, G. P., Bartunik, H. D. & Huber, R. (1999). *Nature (London)*, **400**, 476–480.
Einsle, O., Messerschmidt, A., Huber, R., Kroneck, P. M. H. & Neese, F. (2002). *J. Am. Chem. Soc.* **124**, 11737–11745.
Emsley, P. & Cowtan, K. (2004). *Acta Cryst.* D**60**, 2126–2132.
Fioravanti, E., Vellieux, F. M. D., Amara, P., Madern, D. & Weik, M. (2007). *J. Synchrotron Rad.* **14**, 84–91.
Frankaer, C. G., Mossin, S., Ståhl, K. & Harris, P. (2014). *Acta Cryst.* D**70**, 110–122.
Gabadinho, J. *et al.* (2010). *J. Synchrotron Rad.* **17**, 700–707.
Garman, E. F. (2010). *Acta Cryst.* D**66**, 339–351.
Incardona, M.-F., Bourenkov, G. P., Levik, K., Pieritz, R. A., Popov, A. N. & Svensson, O. (2009). *J. Synchrotron Rad.* **16**, 872–879.
Kabsch, W. (2010). *Acta Cryst.* D**66**, 125–132.
Karplus, P. A. & Diederichs, K. (2012). *Science*, **336**, 1030–1033.
Kemp, G. L., Clarke, T. A., Marritt, S. J., Lockwood, C., Poock, S. R., Hemmings, A. M., Richardson, D. J., Cheesman, M. R. & Butt, J. N. (2010). *Biochem. J.* **431**, 73–80.
Kmetko, J., Husseini, N. S., Naides, M., Kalinin, Y. & Thorne, R. E. (2006). *Acta Cryst.* D**62**, 1030–1038.
Komori, H., Sugiyama, R., Kataoka, K., Miyazaki, K., Higuchi, Y. & Sakurai, T. (2014). *Acta Cryst.* D**70**, 772–779.
Leal, R. M. F., Bourenkov, G., Russi, S. & Popov, A. N. (2013). *J. Synchrotron Rad.* **20**, 14–22.
Leal, R. M. F., Bourenkov, G. P., Svensson, O., Spruce, D., Guijarro, M. & Popov, A. N. (2011). *J. Synchrotron Rad.* **18**, 381–386.
Murshudov, G. N., Skubák, P., Lebedev, A. A., Pannu, N. S., Steiner, R. A., Nicholls, R. A., Winn, M. D., Long, F. & Vagin, A. A. (2011). *Acta Cryst.* D**67**, 355–367.
Nurizzo, D., Mairs, T., Guijarro, M., Rey, V., Meyer, J., Fajardo, P., Chavanne, J., Biasci, J.-C., McSweeney, S. & Mitchell, E. (2006). *J. Synchrotron Rad.* **13**, 227–238.
Owen, R. L., Rudiño-Piñera, E. & Garman, E. F. (2006). *Proc. Natl Acad. Sci. USA*, **103**, 4912–4917.
Paithankar, K. S., Owen, R. L. & Garman, E. F. (2009). *J. Synchrotron Rad.* **16**, 152–162.
Polyakov, K. M., Boyko, K. M., Tikhonova, T. V., Slutsky, A., Antipov, A. N., Zvyagilskaya, R. A., Popov, A. N., Bourenkov, G. P., Lamzin, V. S. & Popov, V. O. (2009). *J. Mol. Biol.* **389**, 846–862.
Schlichting, I., Berendzen, J., Chu, K., Stock, A. M., Maves, S. A., Benson, D. E., Sweet, R. M., Ringe, D., Petsko, G. A. & Sligar, S. G. (2000). *Science*, **287**, 1615–1622.
Sjögren, T. & Hajdu, J. (2001). *J. Biol. Chem.* **276**, 13072–13076.
Sutton, K. A., Black, P. J., Mercer, K. R., Garman, E. F., Owen, R. L., Snell, E. H. & Bernhard, W. A. (2013). *Acta Cryst.* D**69**, 2381–2394.
Tikhonova, T. V., Slutsky, A., Antipov, A. N., Boyko, K. M., Polyakov, K. M., Sorokin, D. Y., Zvyagilskaya, R. A. & Popov, V. O. (2006). *Biochim. Biophys. Acta*, **1764**, 715–723.
Trofimov, A. A., Polyakov, K. M., Boyko, K. M., Tikhonova, T. V., Safonova, T. N., Tikhonov, A. V., Popov, A. N. & Popov, V. O. (2010). *Acta Cryst.* D**66**, 1043–1047.
Trofimov, A. A., Polyakov, K. M., Tikhonova, T. V., Tikhonov, A. V., Safonova, T. N., Boyko, K. M., Dorovatovskii, P. V. & Popov, V. (2012). *Acta Cryst.* D**68**, 144–153.
Weik, M., Ravelli, R. B. G., Kryger, G., McSweeney, S., Raves, M. L., Harel, M., Gros, P., Silman, I., Kroon, J. & Sussman, J. L. (2000). *Proc. Natl Acad. Sci.* **97**, 623–628.
Winn, M. D. *et al.* (2011). *Acta Cryst.* D**67**, 235–242.